randomly distributed, the scattering is approximated using incoherent power addition. Because g varies with the spatially dependent pump power, these equations have no general analytic solution. To simplify the problem, let g be constant (using the spatial average of $P(z)$ and a small pump absorption approximation) so that eqn. 10 may be readily solved. The small spontaneous emission terms have been omitted from eqn. 10, and to arrive at a solution it is assumed that there are small and equal noise source inputs at both ends of the amplifier. In this case, the solutions then have exponent eigenvalues $q_{1,2} = \pm\sqrt{[g^2 - \kappa^2]} \equiv \pm q$ and a denominator term equal to $(q - g)/\kappa \exp(qL) + 1$. The oscillation threshold condition occurs when this denominator approaches zero. For small κ, after expanding the square root, the Rayleigh-induced Raman oscillation condition becomes

$$\frac{\exp(gL)}{gL} = \frac{2}{\kappa L} \tag{11}$$

The back-scatter coefficient can be written as the product of a back-scattering capture factor [10] times the Rayleigh scattering attenuation coefficient, $\kappa \simeq S\alpha_R$. For a good approximation, for very high quality fibres, the Rayleigh scattering attenuation coefficient is taken to be about the same as the total absorption coefficient (in our example, 0.078km^{-1}). The capture factor for typical fibres is in the range $0.210(n_1^2 - n_2^2)/n_1^2 \leq S \leq 0.235(n_1^2 - n_2^2)/n_1^2$. For our fibre example, $S \simeq 1.7 \times 10^{-3}$, giving $\kappa \simeq 1.33 \times 10^{-4}$km^{-1}. Numerical evaluation of eqn. 11 for our example, for lengths from 0–20km, shows that the self-oscillation parameter $g_{Rm}P_pL_{eff}$ is in the range from 9 – 12, less than the previous criterion, 16. The use of the effective length here results from our replacing the spatially dependent gain with its constant spatial average value, to allow for absorption effects. Maximum gains from 41.6 to 50dB for lengths < 10km are predicted for our example. For example, if the amplifier length is 10km, the maximum input power is 2.56W, providing a gain of 41.6dB. Conversely, if the input power is 2W, the maximum amplifier length is 15.0km, providing a maximum gain of 39.6dB. In practice, if such high gains are required, amplifiers should be designed with separate stages separated by optical isolators, to suppress feedback not only from Rayleigh scattering but weak external reflections as well.

Another interesting semi-analytic result can be obtained for a case not using the requirement of constant $g(z)$. If the Raman gain is not assumed to be constant, eqn. 10 can be put in the form

$$\frac{d^2P_f}{dz^2} = \left(\frac{dg}{dz} + g^2 - \kappa^2\right) P_f \tag{12}$$

This also has no general closed-form solution, but if the term in parentheses is constant, has the same sort of exponential solutions found above. To make that term constant, the spatial dependence of the gain must be

$$g(z) = g_0[(e^{2g_0z} - 1)/(e^{2g_0z} + 1)] \tag{13}$$

which for backward pumping is qualitatively very similar to the gain profile resulting from complete absorption of the pump over the amplifier length. The parameter g_0 is then the peak Raman gain at the pump input of the amplifier. The eigenvalue $q = \sqrt{[g_0^2 - \kappa^2]}$, and the same threshold condition as derived above applies, with g_0 taking the place of g and the effective length L_{eff} becoming the actual length, L.

In summary, a new exact analysis of the small-signal gain and noise figure for a counter-pumped fibre Raman amplifier has been presented. The analysis does not require that signal and pump absorption coefficients be equal, but the resulting expressions greatly simplify if they are equal. In addition, new expressions are derived for the stimulated Raman oscillation condition caused by Rayleigh back-scattering, which show thresholds less than the usual condition with no scattering.

Acknowledgments: This work was conducted under the auspices of the Consortium on Wideband All-Optical Networks with full support by the Advanced Research Projects Agency. Opinions, interpretations, conclusions, and recommendations are those of the author and are not necessarily endorsed by the US Air Force.

11 February 1997

Electronics Letters Online No: 19970428

S.R. Chinn (*Lincoln Laboratory, Massachusetts Institute of Technology, 244 Wood Street, Lexington, MA 02173-9108, USA*)

References

1 CHERNIKOV, S.V., ZHU, Y., KASHYAP, R., and TAYLOR, J.R.: 'High-gain, monolithic, cascaded fibre Raman amplifier operating at 1.3μm', *Electron. Lett.*, 1995, **31**, pp. 472–473

2 HANSEN, P.B., STENTZ, A.J., ESKILDEN, L., GRUBB, S.G., STRASSER, T.A., and PEDRAZZANI, J.R.: 'High sensitivity 1.3μm optically preamplified receiver using Raman amplification', *Electron. Lett.*, 1996, **32**, pp. 2164–2165

3 AUYEUNG, J., and YARIV, A.: 'Spontaneous and stimulated Raman scattering in long low loss fibers', *IEEE J. Quantum Electron.*, 1978, **14**, pp. 347–352

4 DAKSS, M.L., and MELMAN, P.: 'Amplified spontaneous Raman scattering and gain in fiber Raman amplifiers', *J. Lightwave Technol.*, 1985, **LT-3**, pp. 806–813

5 VILHELMSSON, K.: 'Simultaneous forward and backward Raman scattering in low-attenuation single-mode fibers', *J. Lightwave Technol.*, 1986, **LT-4**, pp. 400–404

6 SIDDIQUI, A.S., and VIENNE, G.G.: 'The effect of pump and signal laser fluctuations on the output signal from Raman and Brillouin optical fiber amplifiers', *J. Opt. Commun.*, 1992, **13**, pp. 33–36

7 DESURVIRE, E.: 'Erbium-doped fiber amplifiers' (John Wiley & Sons, New York, 1994), Secs. 2.2–2.4

8 MAHGEREFTEH, D., BUTLER, D.L., GOLDHAR, J., ROSENBERG, B., and BURDGE, G.L.: 'Technique for measurement of the Raman gain coefficient in optical fibers', *Opt. Lett.*, 1996, **21**, pp. 2026–2028

9 AGRAWAL, G.P.: 'Nonlinear fiber optics' (Academic Press, New York, 1989), Sec. 8.1

10 BRINKMEYER, E.: 'Analysis of the back-scattering method for single-mode optical fibers', *J. Opt. Soc. Am.*, 1980, **8**, pp. 1010–1012

Azimuthal instabilities and self-breaking of beams into sets of solitons in bulk second-harmonic generation

L. Torner and D.V. Petrov

Indexing terms: Optical harmonic generation, Solitons

The authors investigate numerically the process of second-harmonic generation of light in bulk quadratic nonlinear media with input beams containing phase dislocations. The authors find that above a threshold light intensity, the input beams self-split into several pieces along the azimuthal direction and form sets of spatial solitons.

Introduction: The cascading of second-order nonlinearities has been identified as a new rich source of all-optical phenomena, with important potential applications to the manipulation of light beams and signals [1]. One important example is the formation of spatial solitons which, under conditions for second-harmonic generation (SHG), form by the mutual trapping and locking together of the fundamental and second-harmonic beams. The dynamics on evolution of the solitons holds promise for different applications, which include beam steering, scanning and switching, and the existence and excitation of solitons can strongly affect the wave evolution in quadratic media in different geometries and generate new opportunities for the control of light. To explore this possibility, in this Letter we address the process of SHG in bulk crystals with intense beams containing phase dislocations. We find that the beams exhibit azimuthal instabilities and as a consequence self-split into several pieces and form sets of solitons.

Evolution equations: We consider CW light beams travelling in a medium with a quadratic nonlinearity under conditions for type I second-harmonic generation. In the slowly-varying envelope approximation, the beam evolution can be described by the normalised equations [2]

$$\begin{aligned} i\frac{\partial a_1}{\partial \xi} - \frac{r}{2}\nabla_\perp^2 a_1 + a_1^* a_2 \exp(-i\beta\xi) = 0 \\ i\frac{\partial a_2}{\partial \xi} - \frac{\alpha}{2}\nabla_\perp^2 a_2 - i\delta\hat{\delta}\cdot\nabla_\perp a_2 + a_1^2 \exp(i\beta\xi) = 0 \end{aligned} \tag{1}$$

where a_1 and a_2 are the amplitudes of the fundamental and second-harmonic waves, $r = -1$, and $\alpha = -k_1/k_2$. Here $k_{1,2}$ are the linear wavenumbers at both frequencies. The parameter β is given by $\beta = k_1\eta^2\Delta k$, where $\Delta k = 2k_1 - k_2$, is the wavevector mismatch and η is a beamwidth. The parameter δ accounts for Poynting vector walk-off and is given by $\delta = k_1\eta\rho$, ρ being the walk-off angle. In eqn. 1 the transverse co-ordinates are in units of η, and the scaled propagation co-ordinate is $\xi = z/k_1\eta^2$.

Input conditions: To examine the new phenomena present in the process of SHG with input beams having phase dislocations, we performed series of numerical experiments solving eqn. 1 with a split-step Fourier algorithm for a variety of conditions. We present the results obtained with Gaussian input beams having a phase dislocation nested in the centre, namely $a_1(\xi = 0) = Ar_\perp^{|m|} \exp(im\varphi) \exp(-r_\perp^2/w^2)$, where φ is the azimuthal angle in cylindrical co-ordinates, m the topological charge of the dislocation, and $\mathrm{sgn}(m)$ its chirality. In all the results shown here we set $w = 2$. The phase dislocation can be generated experimentally in different ways, e.g. with appropriate phase masks. To seed any instabilities present in the system, we considered noise fluctuations in the input light so that we multiplied the input by the factor $[1+R(r_\perp)]$, where R is a uniformly distributed, complex random quantity with $\langle R\rangle = 0$ and $\langle|R|\rangle = \sigma$. We set $\sigma = 10^{-2}$, and verified that the relevant results do not depend on that choice.

Azimuthal-beam breaking into solitons: Our primary goal is to uncover the impact of the phase dislocation in the beam evolution and we focus on the case $m = 1$. In our simulations we observed that below a threshold power the fundamental input creates a second-harmonic beam and then both beams spread due to diffraction. However, we found that above the threshold, the beams self-break along the azimuthal direction into several subbeams that then self-trap and form sets of solitons. The self-breaking of the beams was found to occur for a wide range of input light powers and material conditions.

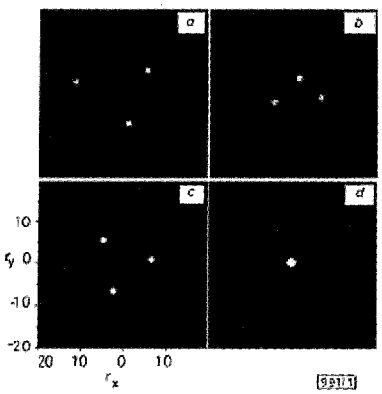

Fig. 1 *Fundamental beam at propagation co-ordinate $\xi = 10$ for different conditions*

Features are similar for SH beam and thus not shown
a $A = 8$, $\beta = 0$, $m = 1$
b $A = 6$, $\beta = 0$, $m = 1$
c $A = 6$, $\beta = 3$, $m = 1$
d $A = 4$, $\beta = 0$, $m = 0$
In all cases $\delta = 0$

Fig. 1 shows a summary of the outcome of series of illustrative simulations in the absence of Poynting vector walk-off. Figs. 1*a* and *b* correspond to phase-matching and two different input light powers, and in Fig. 1*c* we set $\beta = 3$, which is representative of the beam evolution at positive wavevector mismatch. Simulations with different noise realisations produce different output patterns but we always observed the same number of solitons, namely three solitons in the conditions of Figs. 1*a–c*. The wave evolution at negative β is drastically different and the beams spread, because at $\beta < 0$ a much higher input power is required to form solitons without a strong second-harmonic initial seed [2]. When the input is a beam without the phase dislocation only one soliton is formed as shown in Fig. 1*d*.

The spontaneous beam breaking can be attributed to the azimuthal instability of the ring-shaped beams, related to the modulational instability of plane-wave eigenmodes in quadratic nonlinear media [3, 4], and analogous to the azimuthal-symmetry breaking of ring-shaped beams in saturable cubic nonlinear media [5, 6]. We observed that ring-shaped beams without the phase dislocation tend to break into several subbeams but those attract each other and merge to a single output soliton. However, with the phase dislocation the input light carries angular momentum.

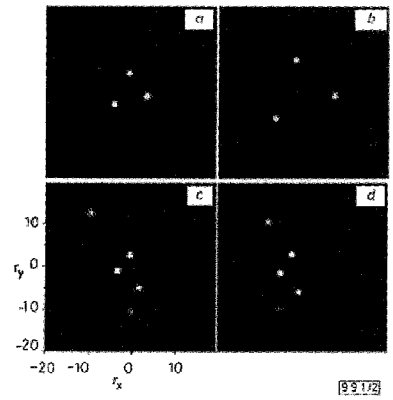

Fig. 2 *Detail of evolution of output solitons during propagation and with Poynting vector walk-off*

a, *b* Without Poynting vector walk-off
c, *d* With Poynting vector walk-off
Conditions: $A = 6$, $\beta = 0$, $m = 1$
In *a* and *b*: $\delta = 0$; in *c*: $\delta_x = 0.5$; in *d*: $\delta_x = 1$. In *a*, *c*, *d*: $\xi = 10$; in *b*: $\xi = 15$

As a consequence, the output solitons acquire different relative phases and different linear momenta, thus they move apart and separate from each other during propagation, as shown in Figs. 2*a* and *b*. Notice that Fig. 2*a* and 1*b* are not identical because they correspond to different noise realisations. The effects introduced by the existence of Poynting vector walk-off are illustrated in Figs. 2*c* and *d*. Walk-off breaks the azimuthal symmetry of the system and therefore modifies the pattern of output light. In particular, with walk-off the pattern of output solitons is the same for all numerical noise realisations. We verified that an alternative way to control the pattern of the output light is the presence of a weak second-harmonic input signal.

Conclusions: We addressed numerically the SHG of light in bulk quadratic nonlinear media. We found the azimuthal-beam breaking into sets of spatial solitons of intense input beams containing phase dislocations. The pattern of output light depends on the material and input light conditions, in particular the input power and the topological charge of the phase dislocations, and it can be controlled, for example, by the presence of a coherent SH seed.

Acknowledgments: This work has been partially supported by the Spanish Government under grant PB95-0768.

20 January 1997
Electronics Letters Online No: 19970429

L. Torner and D.V. Petrov (*Department of Signal Theory and Communications, Universitat Politecnica de Catalunya, Gran Capitan UPC-D3, Barcelona, ES 08034, Spain*)

D.V. Petrov: Permanent address: Institute of Semiconductor Physics, Novosibirsk, 630090, Russia

References

1 STEGEMAN, G.I., HAGAN, D.J., and TORNER, L.: '$\chi^{(2)}$ cascading phenomena and their applications to all-optical signal processing, mode-locking, pulse compression and solitons', *Opt. Quantum Electron.*, 1996, **28**, pp. 1691–1740

2 TORNER, L., and WRIGHT, E.M.: 'Soliton excitation and mutual locking of light beams in bulk quadratic nonlinear crystals', *J. Opt. Soc. Am. B*, 1996, **13**, pp. 864–875

3 TRILLO, S., and FERRO, P.: 'Modulational instability in second-harmonic generation', *Opt. Lett.*, 1995, **20**, pp. 438–440

4 KANASHOV, A.A., and RUBENCHIK, A.M.: 'On diffraction and dispersion effect on three wave interaction', *Physica D*, 1981, **4**, pp. 122–134

5 SOTO-CRESPO, J.M., WRIGHT, E.M., and AKHMEDIEV, N.N.: 'Recurrence and azimuthal-symmetry breaking of a cylindrical Gaussian beam in a saturable seff-focusing medium', *Phys. Rev. A*, 1992, **45**, pp. 3168–3175

6 TIKHONENKO, V., CHRISTOU, J., and LUTHER-DAVES, B.: 'Spiraling bright spatial solitons formed by the breakup of an optical vortex in a saturable self-focusing medium', *J. Opt. Soc. Am. B*, 1995, **12**, pp. 2046–2052

Nonlinear fibre-optic receiver for ultrashort pulse code division multiple access communications

H.P. Sardesai and A.M. Weiner

Indexing terms: Optical receivers, Multi-access systems, Optical communication

The authors present experimental results on a nonlinear optical receiver for ultrashort pulse code division multiple access communications which uses nonlinear frequency shift effects in optical fibres to perform intensity discrimination with femtosecond response times. The receiver exhibits a contrast ratio of nearly 1000 for received pulse energies of ~1pJ.

Optical code division multiple access (CDMA) communication systems are an interesting choice for local area optical networks due to their unique attributes of optical processing, asynchronous transmission, high information security and multiple access capability [1]. In a previously proposed optical CDMA scheme using coherent ultrashort pulses [1, 2], the CDMA transmitters would use a spectral phase encoder to convert input femtosecond pulses into low intensity pseudonoise bursts. Multiple-access would be accomplished by assigning different, minimally interfering phase codes to different users. Correctly coded signals are converted back into femtosecond pulses by a spectral phase decoder in the CDMA receiver, while incorrectly coded signals remain as low intensity pseudonoise bursts. The desired data can be then detected using a nonlinear optical thresholder. The key requirement for the ultrashort pulse CDMA receiver/thresholder is the ability to discriminate between properly decoded femtosecond pulses and the equally energetic but improperly decoded picosecond interference signals. In this Letter we report on a nonlinear fibre-optic receiver for an ultrashort pulse optical CDMA system which uses intensity dependent nonlinear frequency shift effects in optical fibres to achieve thresholding with a high contrast ratio approaching 1000.

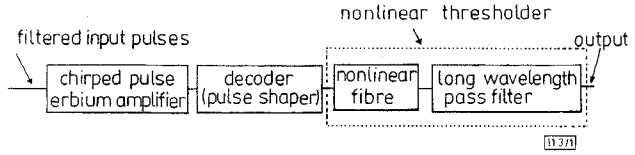

Fig. 1 *Block diagram of experimental arrangement*

A block diagram of the receiver is shown in Fig. 1. Input pulses to the experiment are generated by a stretched pulse modelocked fibre ring laser [3] and are spectrally filtered to yield pulse durations of ~275fs with a repetition rate of 31.2MHz, an average power 30μW and a bandwidth of ~11nm centred at ~1559nm. These pulses are amplified by a chirped pulse erbium doped fibre amplifier. In the amplifier, input pulses are first stretched by propagating them through 60m of standard singlemode fibre. They are then propagated through 26m of erbium doped fibre (Corning type II T-8533-301) which serves as the gain medium and are finally compressed by 13.4m of dispersion compensating fibre (AT&T fibre JR1DC1074C10C). When pumped by 130mW of pump power at 980nm, the amplifier exhibits a gain of ~29dB and an output power of ~20mW. Gain narrowing in the amplifier broadens the pulses to between 350 and 500fs with a corresponding spectral bandwidth of 6–8nm centred at 1559nm. At output powers higher than ~5mW, in addition to gain narrowing we see some small nonlinear effects in the compressed pulses as evidenced by some broadening at the base of the pulses in the autocorrelation traces. Overall, the output pulses are close to distortion free with measured FWHM time-bandwidth products between 0.32 to 0.36 for output powers between ~4 to ~15mW. The amplified pulses are then passed through a fibre pigtailed pulse shaper containing a 128 element liquid crystal phase modulator (LCM) which acts as a programmable spectral encoder [4]. As demonstrated before [4], in the pulse shaper, the LCM is used to set the spectral phases either to a length 63 M-sequence pseudorandom phase code (which encodes the pulses into 10–12ps wide pseudorandom bursts) or held constant (leading to 600–800fs uncoded pulses). For *M*-sequence bits equal to 1, the phases of the corresponding LCM pixels are set to π radians; for bits equal to zero, the phase is set to 0 radians. The entire *M*-sequence is accommodated by the LCM with two pixels of the LCM corresponding to every bit of the *M*-sequence. The insertion loss of the entire pulse shaper from the input fibre to the output fibre is ~8.8dB. For a full CDMA system consisting of an encoder and a decoder, the coded pulse here would correspond to an improperly decoded signal in the full system; the uncoded pulses would similarly correspond to properly decoded pulses in the full system. Although ideally a pulse shaper should cause no temporal pulse broadening when a constant phase is applied to the LCM [4], we do observe some broadening for the uncoded pulses here; the cause of this broadening is currently under investigation.

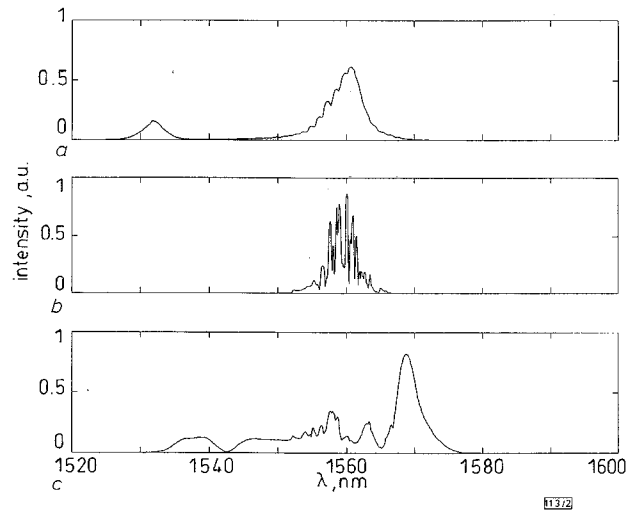

Fig. 2 *Power spectra*

a At input of decoder
b Coded signal (which would be equivalent to improperly decoded signal for full system with both encoders and decoders) at output of thresholder
c Uncoded signal (which would be equivalent to properly decoded signal for full system with both encoders and decoders) at output of thresholder
Average power at input of receiver is 30μW and average power at input of nonlinear thresholder fibre is 0.44mW for *b* and *c*

Coded or uncoded pulses from the pulse shaper are connected to the nonlinear thresholder which is simply a 500m length of dispersion shifted optical fibre with zero dispersion wavelength $\lambda_0 \simeq$ 1559nm (which is near the centre of the amplified spectrum) followed by a longpass filter and photodetector. Nonlinear propagation effects cause the spectrum of the uncoded pulse to split and spread to either side of λ_0 [5, 6]. The magnitude of the spectral split can be controlled by varying the intensity and time duration of the pulse and the propagation distance through the fibre. The coded pulse with a lower intensity and larger time duration propagates through the same length of the thresholder fibre but exhibits negligible spectral shifts. Figs. 2*b* and *c* shows the power spectral data for 0.44mW average power in the thresholder fibre clearly revealing the differences in the output spectra for coded and uncoded pulses. The power spectrum at the input of the decoder is also shown for comparison in Fig. 2*a*. Please note that the emission at 1530nm and the long wavelength tail at 1570nm of the amplifier output spectrum are suppressed in the pulse shaper due to the finite aperture of the pulse shaper optics. These frequency